Front. Environ. Sci. Eng. 2019, 13(5): 77
https://doi.org/10.1007/s11783-019-1161-0

RESEARCH ARTICLE

Enhanced activation of peroxymonosulfate by CNT-TiO_2 under UV-light assistance for efficient degradation of organic pollutants

Xuemin Hao[1], Guanlong Wang[2], Shuo Chen (✉)[1], Hongtao Yu[1], Xie Quan[1]

1 Key Laboratory of Industrial Ecology and Environmental Engineering (Ministry of Education), School of Environmental Science and Technology, Dalian University of Technology, Dalian 116024, China
2 School of Light Industry and Chemical Engineering, Dalian Polytechnic University, Dalian 116034, China

HIGHLIGHTS

- CNT-TiO_2 composite is used to activate PMS under UV-light assistance.
- Superior performance is due to the enhanced electron-transfer ability of CNT.
- SO_4•$^-$, •OH and $^1O_2$ play key roles in the degradation of organic pollutants.

ARTICLE INFO

Article history:
Received 23 March 2019
Revised 9 August 2019
Accepted 15 August 2019
Available online 28 September 2019

Keywords:
Peroxymonosulfate activation
Carbon nanotubes
TiO_2
Water treatment

GRAPHIC ABSTRACT

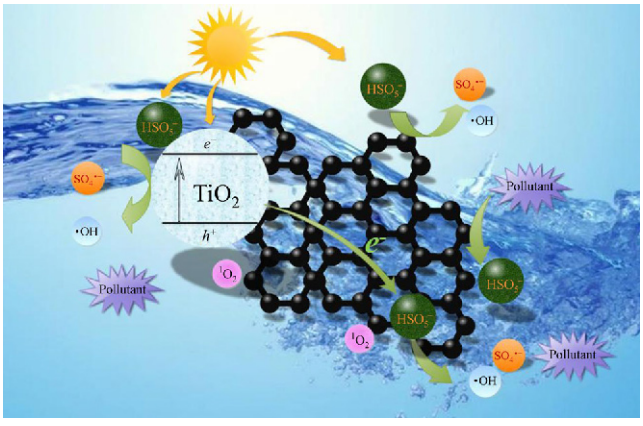

ABSTRACT

In this work, a UV-light assisted peroxymonosulfate (PMS) activation system was constructed with the composite catalyst of multi-walled carbon nanotubes (CNT) - titanium dioxide (TiO_2). Under the UV light irradiation, the photoinduced electrons generated from TiO_2 could be continuously transferred to CNT for the activation of PMS to improve the catalytic performance of organic pollutant degradation. Meanwhile, the separation of photoinduced electron-hole pairs could enhance the photocatalysis efficiency. The electron spin resonance spectroscopy (EPR) and quenching experiments confirmed the generation of sulfate radical (SO_4•$^-$), hydroxyl radical (•OH) and singlet oxygen ($^1O_2$) in the UV/PMS/20%CNT-TiO_2 system. Almost 100% phenol degradation was observed within 20 min UV-light irradiation. The kinetic reaction rate constant of the UV/PMS/20%CNT-TiO_2 system (0.18 min^{-1}) was 23.7 times higher than that of the PMS/Co_3O_4 system (0.0076 min^{-1}). This higher catalytic performance was ascribed to the introduction of photoinduced electrons, which could enhance the activation of PMS by the transfer of electrons in the UV/PMS/CNT-TiO_2 system.

1 Introduction

In recent decades, sulfate radical-advanced oxidation processes (SR-AOPs) have received attention in environmental remediation. Compared with hydroxyl radical (E_0 = 2.8 V), the sulfate radical (SO_4•$^-$) has close or even higher redox potential of 2.5–3.1 V (*vs.* NHE) (Ghanbari and Moradi, 2017). Moreover, sulfate radical has higher selectivity, a longer half-life (30–40 μs) and could be active in a wider reaction pH range (pH = 2–8) than •OH (Yang et al., 2008; Zhao et al., 2017). Generally, the peroxymonosulfate (PMS) can be activated by several methods, such as transition metal ions, homogeneous

✉ Corresponding author
E-mail: shuochen@dlut.edu.cn

transition metal composites, UV and carbonaceous catalyst (Anipsitakis and Dionysiou, 2003; Liang et al., 2012; Lei et al., 2015; Ren et al., 2015). The transition metal catalysts can effectively activate PMS, but there is a risk of inevitable metal leaching, which could cause pollution to the waters again (Zhang et al., 2018). As the non-metal catalyst, carbonaceous catalysts have attracted great interests in the field of PMS activation because of its several attractive features, such as metal-free nature, larger specific surface area, and tunable physicochemical properties (Duan et al., 2015a, 2015b; Wang et al., 2017). In particular, the electron-transfer ability of carbon-based catalysts played an important role in the PMS activation (Duan et al., 2015a, 2016). The researchers have confirmed that CNTs could activate persulfates via nonradical mechanisms that the charges transfer from phenol (e^- donor) to PMS (e^- acceptor) via CNT(e^- mediator) (Lee et al., 2015). However, the activation efficiency of current carbon materials need to be improved. Recently, various methods have been employed to improve the electron-transfer ability of carbonaceous catalysts by changing the electron distribution of catalysts. Doping with heteroatoms, such as S (Guo et al., 2018), N (Guo et al., 2019), and Co/N (Wang et al., 2019), has been found to be an efficient method to improve the electron-transfer ability.

Despite the above progress, more efficient methods are desired to enhance the catalytic degradation performance. The photoactivation of PMS via ultraviolet (UV)-light has advantages of clean and mild reaction conditions, but it suffered from the low activation efficiency. When the photocatalysts were applied directly or as supports for transition metals or metallic oxides, such as ZnO (Shukla et al., 2010), Co-TiO_2 (Chen et al., 2014) and TiO_2@Cu-Fe_2O_4 (Golshan et al., 2018), the activation efficiency of PMS increased obviously in the UV/PMS system. TiO_2 is a non-toxic classical photocatalyst with excellent stability, and was investigated widely in water treatment (Wang et al., 2010; Verma et al., 2016). In the photocatalytic process, when the semiconductors are irradiated by the photons with energy equal to or higher than the band gap energy, the electrons in the valence band will be promoted to the conduction band (Taha et al., 2016; Matafonova and Batoev, 2018). The photoinduced electrons and holes are involved in redox reaction processes.

Inspired by photoinduced electrons, it could be speculated that when the carbon-based PMS activation is integrated with photoactivation of PMS, the photoinduced electrons could be able to intensify the charge transfer for the carbon-based PMS activation. The separation efficiency of electron-hole pairs could be improved. Therefore, the CNT was chosen due to its unique characteristics which are beneficial to persulfate and peroxymonosulfate activation, such as the network of sp^2 covalent carbon, defective sites, and oxygen functional groups (e.g., – COOH, – C = O, and – OH) (Wang and Wang, 2018).

In this study, the UV-light assisted system for the activation of PMS was constructed with CNT-TiO_2 composite prepared by a hydration/dehydration method. Several refractory pollutants including phenol, atrazine (ATZ), sulphamethoxazole (SMZ), and bisphenol A (BPA) were chosen to evaluate the catalytic performance of the UV/PMS/CNT-TiO_2 system. The reactive species generated during the reaction were analyzed by the EPR technique. The catalytic mechanism of PMS activation in the UV/PMS/ CNT-TiO_2 system has also explored.

2 Materials and methods

2.1 Materials

Tetra-n-butyl titanate was purchased from Shanghai Kefeng Chemical Reagent Co., Ltd (China) and ethanol absolute was from Tianjin Dongliqu Tianda Chemical Reagent factory (China). The peroxymonosulfate (Oxone: $2KHSO_5 \cdot KHSO_4 \cdot K_2SO_4$, PMS) was purchased from Aladdin Industrial Corporation (China). Multi-walls carbon nanotubes (purity:>97%, main range of diameter: 20–40 nm, length: 5 μm, special surface area: 80–140 m^2/g) purchased from Shenzhen Nanotech Port Co., Ltd (China). All chemicals were analytical grade and the resistivity of ultrapure water was 18 MΩ·cm in this work.

2.1.1 Preparation of acidified CNT

One g CNT was added to 40 mL of a 3:1 mixture of concentrated sulfuric acid (98 wt.%) and nitric acid (63 wt.%) in a round-bottomed flask and was heated at 80°C for 0.5 h. The acidified CNTs were washed with ultrapure water until achieving a neutral pH and dried at 80°C in the oven.

2.1.2 Preparation of TiO_2

The TiO_2 was prepared via the sol-gel synthesis method (Cao et al., 2010). One g tetra-n-butyl titanate was gently added in 60 mL ethanol solution under vigorously stirring for 30 min at room temperature. Then 1.0 mL ultrapure water was added dropwise into it. The mixture turned into the white floccule liquid after stirring for 2 h. The liquid was washed three times with ethanol and dried in the oven at 80°C. The white powder was converted into anatase in the air at 400°C for 2 h with the heating rate of 2.0°C/min.

2.1.3 Preparation of CNT-TiO_2 composite

The CNT-TiO_2 composites were prepared via a hydration/dehydration approach (Yao et al., 2008). The appropriate amount of CNT was added in ultrapure water. After 10 min ultrasonic dispersion, the desired amount of TiO_2 powder

was added into the CNT suspension. The mixture was dispersed under ultrasonication for 10 min and heated at 80°C with stirring until all water evaporated. Then the composite powders of CNT-TiO_2 were obtained.

2.2 Methods

2.2.1 Characterizations of catalysts

The morphology of composite catalyst was observed by scanning electron microscopes (FE-SEM, S-4800, Hitachi, Japan). The crystal structure of catalysts was characterized using X-ray diffraction (XRD, Smartlab 9, Rigaku, Japan) with Cu Kα radiation (voltage 45 kV, current 200 mA). The specific surface areas and pore size distributions were analyzed with a Quantasorb surface area analyzer (Quadrasorb–SI-1 Quantachrome Corp., USA). The UV/Vis spectrophotometer (V-550, JASCO, Japan) was used to record the diffuse reflectance spectroscopy of the catalysts. The photoluminescence (PL) analysis was carried out with Fluorescence spectrophotometer (FL4500, Hitachi, Japan). Electrochemical impedance spectroscopy (EIS) test was performed to explore electron transfer resistance where occurred at different interfaces of UV/PMS/CNT-TiO_2 system with an electrochemical workstation (CHI660D, Shanghai Chenhua Ltd., China) in a traditional system with the CNT-TiO_2 composite as working electrode, platinum sheet as counter electrode, and saturated calomel electrode (SCE) as reference electrode.

2.2.2 Experimental procedures and analytical methods

The experiment was carried out in the 100 mL beaker with magnetically stirring under the Xenon lamp (UV/Vis light, 300 W, Perfect Light Ltd., China) at 30°C. The surface irradiance is 900 μW/cm^2 measured by irradiation meter (FZ-A, Beijing Normal University, China). The scheme of the reaction device was shown in Fig. 1. The UV-light, power, reactor, stirrer and cooling-system are all placed in the opaque reaction box. First, 0.5 g/L CNT-TiO_2 composite was dispersed in 50 mL phenol solution (10 mg/L). After 30 min adsorption/desorption equilibrium process, the lamp was turned on immediately and the specific amount of PMS was added. At this moment, the reaction started. At the certain time, the 1.0 mL sample was taken from the solution and was filtered with 0.22 μm membrane filter. Meanwhile, the 0.1 mL methanol for quenching radicals remained was mixed with the sample. The effects of different content of the CNT in composite, initial pH, composite catalysts dosage and the molar ratio of phenol/PMS were investigated. The catalytic performance of the UV/PMS/CNT-TiO_2 system was evaluated by the degradation of phenol and other organic compounds, including atrazine (ATZ), sulphamethoxazole (SMZ), and bisphenol A (BPA).

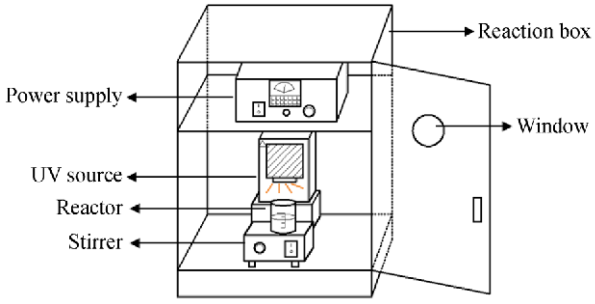

Fig. 1 The scheme of the reaction device.

The concentrations of phenol were measured by the high performance liquid chromatography (HPLC, Waters 2695, USA) with the C18 column at its maximum absorption wavelength of 271 nm. The mobile phase was methanol/water mixture (70:30, v/v) at the flow rate of 1.0 mL/min. The radicals generated during the reaction were detected by EPR spectrometer (Bruker A200, Germany) with the spin-trapping agent of 5,5-dimethyl-pyrroline N-oxide (DMPO) and 2,2,6,6-tetramethyl-4-piperidinol (TMP). The DMPO/TMP was prepared with ultrapure water at a concentration of 50 mmol/L. The conditions of EPR experiment were as follows: microwave frequency, 9.52 GHz; modulation frequency, 100 kHz; center field, 3385 G; sweep width, 200 G and power of 2.01 mW.

3 Results and discussion

3.1 Characterization of CNT-TiO_2

As shown in Figs. 2 (a) and 2(b), the acidified CNTs illustrated a network of continuous fibers and the TiO_2 presented in oval or round shapes. For the CNT-TiO_2

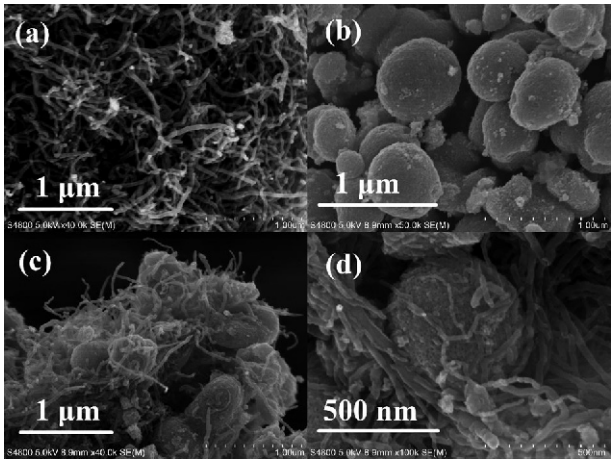

Fig. 2 The surface morphology images of CNT (a), TiO_2 (b) and 20% CNT-TiO_2 composite catalysts (c) with its details (d).

composite with 20% content of CNT,CNT bundles are well dispersed and interwoven among TiO_2 particles as shown in Figs. 2(c) and 2(d). Eventually, the composite can form a good network with CNT fibers and TiO_2 particles for enhancing the transfer of electrons.

As shown in Table 1, the specific surface area of pure TiO_2, CNT and CNT-TiO_2 composites with different CNT content was in the range of 78–96 m^2/g. The variation of specific surface area had little influence on the adsorption and desorption equilibrium, with about 10% of phenol adsorbed within 30 min.

Table 1 Specific surface properties and pore volume of TiO_2, CNT and composites

CNT content in CNT-TiO_2 composite (wt. %)	S_{BET} (m^2/g)	V (cm^3/g)
0	84.391	0.249
5	78.741	0.224
10	81.584	0.229
20	95.905	0.253
30	89.347	0.236
40	96.255	0.243
100	85.949	0.218

The pore-size distributions of composites were analyzed by Barrett-Joyner-Halenda (BJH) method. The pores approximately distributed in the mesoporous range of 2–8 nm (Fig. 3). The mesoporous structure of composites may facilitate the mass transferring during catalytic reaction (Hu et al., 2011).

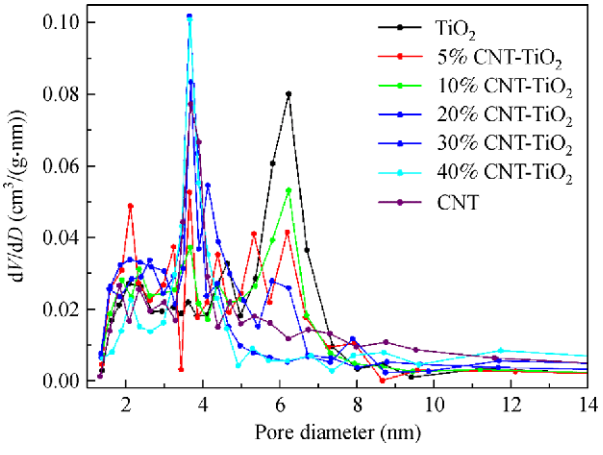

Fig. 3 The pore distribution of the catalysts which based on their nitrogen desorption curves.

The UV-Vis spectra and X-ray diffraction patterns of the TiO_2, CNT and composites of different CNT content were shown in Fig. 4. The wavelength range of UV-light was set at 200–800 nm to observe the light absorption properties of the TiO_2, CNT and CNT-TiO_2 composites of different CNT content. As shown in Fig. 4(a), the TiO_2 alone could be excited evidently by the UV-light (<380 nm) while the CNT showed a light absorption in the full light region owing to its black nature. For the composites, the absorption peaks exhibited obvious red-shift slightly. The enhanced light absorption could be attributed to the combination of TiO_2 and CNT.

The X-ray diffraction patterns of TiO_2, CNT and composites of different CNT content were shown in Fig. 4(b). The characteristic diffraction peaks of CNT located at around 26° and 43°, which could be assigned to carbon (002) and (100) diffractions (Yu et al., 2007). According to PDF-#21.1272, the broad peaks of prepared TiO_2 located at around 25°, 38°, 48°, 54°, 55° and 63°, corresponding to the anatase type TiO_2. For the composites with different CNT content, their characteristic peaks were the same as those of the pure TiO_2, meaning the crystal structure of TiO_2 was not affected by the addition of CNT. Nevertheless, the peaks of CNT were not observed, which is probably attributed to two aspects. One is the small amount of CNT content; another one is the main characteristic peak of CNT at 26° may be overlapped by the peak at 25° of anatase TiO_2. The results were similar with others' researches (Zhang et al., 2010; Zhang et al., 2011; Yang et al., 2013).

3.2 Catalytic performance of UV/PMS/CNT-TiO_2

The catalytic performance of the UV/PMS/20%CNT-TiO_2 system was investigated by the degradation of phenol. Figure 5(a) showed that nearly 10% of phenol was removed within 30 min of adsorption on composite catalysts. For UV/PMS and PMS/20%CNT-TiO_2 system, the phenol removal was 37.5% and 13.1% during 60 min, respectively, which attributed to the oxidation by sulfate and hydroxyl radical generated or via nonradical pathway. It is noteworthy that almost 100% of phenol was degraded within 20 min in the UV/PMS/20%CNT-TiO_2 system. The reaction kinetic rate constant was 0.18 min^{-1}, which was 2.6 times that of the UV/PMS/TiO_2 system (0.068 min^{-1}) (Fig. 5(b)). After 60 min of reaction, the PMS/Co_3O_4 system could remove only 42.3% of phenol with rate constant of 0.0076 min^{-1}, which is much lower than that of the UV/PMS/20%CNT-TiO_2 system. For comparison, the results of some experiments were shown in Fig. 6.

Moreover, Fig. 7 showed the good performance of the UV/PMS/20%CNT-TiO_2 system for the degradation of other refractory pollutants, such as ATZ, SMZ, and BPA. ATZ and SMZ were almost completely removed within 40 min. The degradation of SMZ was more efficient than that of phenol in the UV/PMS/20%CNT-TiO_2 system. Although the BPA removal was 90% in 40 min, 40% of BPA was removed by adsorption before the catalytic degradation. The different degradation trends may be due to the different selectivity of radicals for different pollutants.

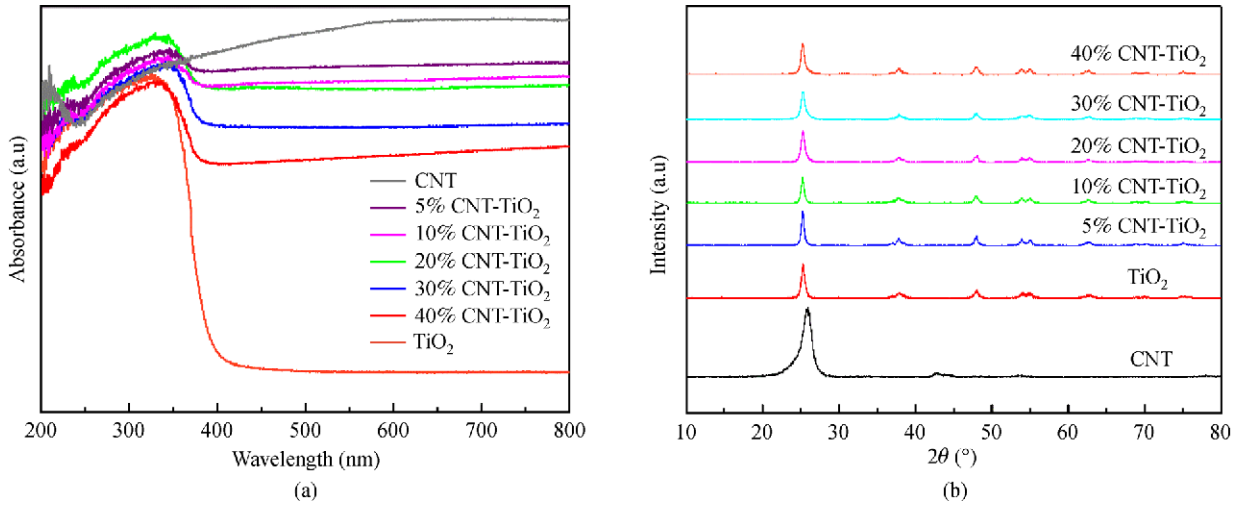

Fig. 4 The UV-Vis spectra (a) and the X-ray diffraction pattern (b) of the TiO_2, CNT and CNT-TiO_2 composites of different CNT content.

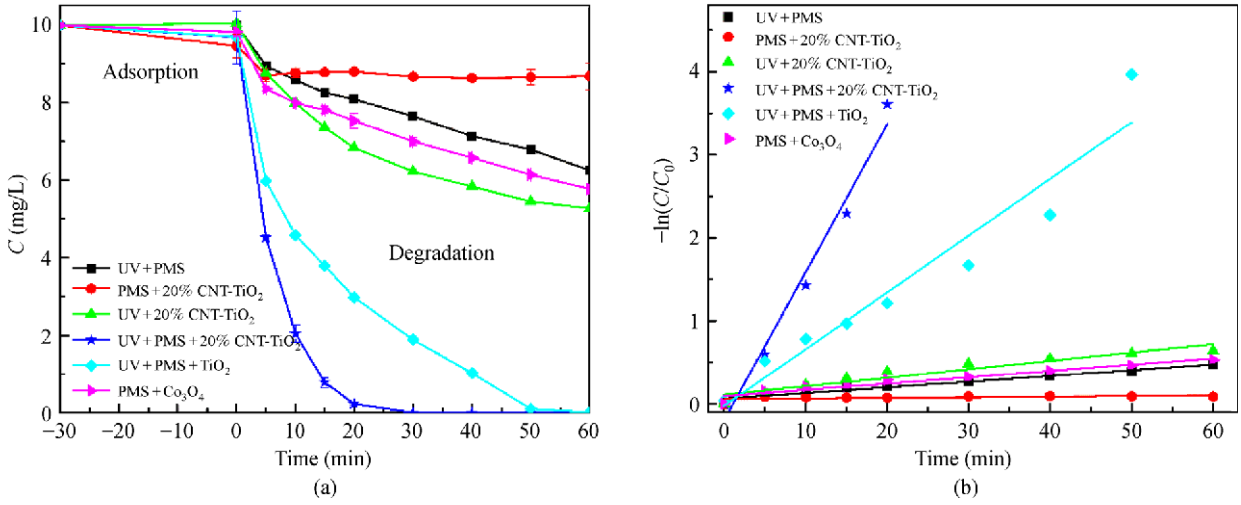

Fig. 5 The phenol removal (a) and kinetic rates of phenol degradation (b) in various reaction systems. ([phenol] = 10 mg/L, [catalyst] = 0.5 g/L, the molar ratio of phenol/PMS = 1:16, initial pH = 6.98, t = 30°C).

3.3 Effects of reaction parameters on the performance UV/PMS/CNT-TiO_2 system

The effect of several key parameters was investigated on the catalytic performance of UV/PMS/CNT-TiO_2 system, including different doping amounts of CNT in composite, initial pH, composite catalyst dosage and the molar ratio of phenol/PMS.

The influence of different CNT content in composite for the phenol degradation was shown in Fig. 8(a). With the increase of CNT content in composites from 5% to 20%, the degradation efficiency of phenol increased gradually. The phenol degradation followed the pseudo-first-order kinetic. In particular, the rate constant increased from 0.066 min^{-1} at 5% doping amount of CNT to 0.18 min^{-1} at 20% doping amount of CNT. The proper doping amount of CNT in composite could enhance the separation efficiency of electron-hole pairs to increase the electrons in the PMS activation by the transferring from TiO_2 to PMS. However, when the CNT content further increased to 40%, the rate constant of phenol degradation decreased to 0.041 min^{-1} in the UV/PMS/CNT-TiO_2 system. This phenomenon maybe ascribed to the cover of surface of TiO_2 by excess CNT in composite, which would hinder the absorption of UV light and reduce the efficiency of phenol degradation. Thus, 20% doping amount of CNT in the composite was optimal content for efficient degradation of phenol in the UV/PMS/CNT-TiO_2 system.

As shown in Fig. 8(b), the UV/PMS/CNT-TiO_2 system can effectively remove phenol at the initial pH range from 3.19 to 9.13. It is noted that the phenol was almost completely removed in 20 min at initial pH of 6.98, which was similar to the phenol removal at initial pH of 5.02 and initial pH of 9.13. Moreover, at initial pH of 3.19, the

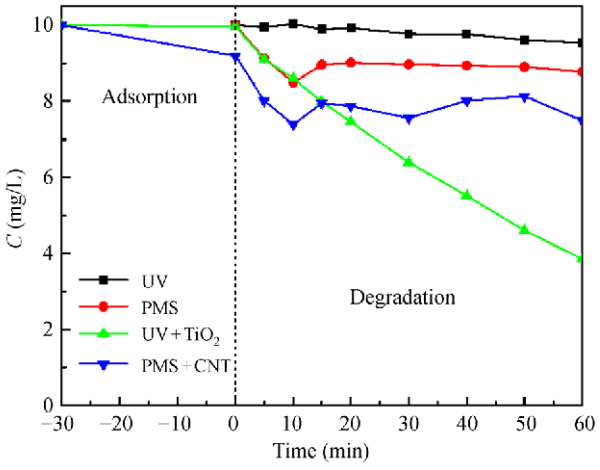

Fig. 6 The phenol removal in the UV, PMS, UV/TiO_2 and PMS/CNT systems. ([phenol] = 10 mg/L, [catalyst] = 0.5 g/L, the molar ratio of phenol/PMS = 1:16, initial pH = 6.98, t = 30°C).

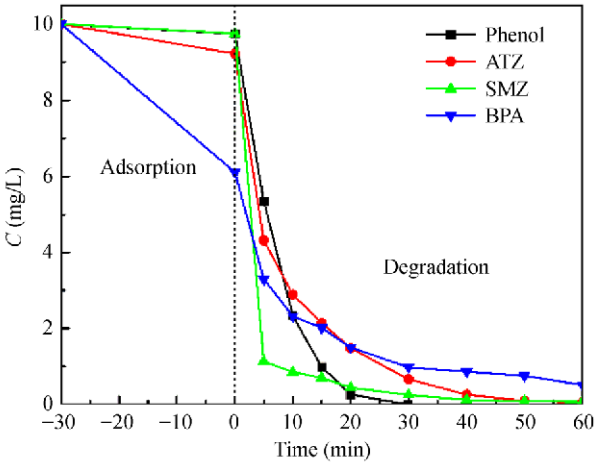

Fig. 7 Degradation of different pollutants by UV/PMS/20% CNT-TiO_2 system. ([pollutant] = 10 mg/L, [catalyst] = 0.5 g/L, the molar ratio of pollutant/PMS = 1:16, initial pH = 6.98, t = 30°C).

phenol removal was slightly higher and the phenol was degraded within 15 min reaction time. The results suggested that the initial pH had little effect on the degradation efficiency of the pollutants in the UV/PMS/CNT-TiO_2 system, which was consistent with Dikdim's work (Dikdim et al., 2019).

Figure 8(c) showed the effect of catalyst dosage for phenol degradation. When the 20%CNT-TiO_2 dosage was 0.1 g/L, the removal efficiency of phenol was about 90% within 60 min. With the increase of catalyst dosage (0.3, 0.5 or 0.7 g/L), the phenol could be removed totally in 30 min. However, when the composite dosage increased to 0.7 g/L, the removal efficiency of phenol decreased slightly in 20 min, which suggested the excessive dosage was unfavorable for the light absorption, which lower the catalytic performance of the system.

The molar ratio of phenol/PMS also plays an important role in the degradation of phenol. As shown in Fig. 8(d), the rate constant of the phenol degradation increased from 0.062 min^{-1} at the molar ratio of 1:4 (phenol/PMS) to 0.082 min^{-1} at the molar ratio of 1:8 (phenol/PMS). At the molar ratio of 1:16 (phenol/PMS), the rate constant of phenol degradation was 0.18 min^{-1}, being 2.17 times that of the molar ratio of 1:8 (phenol/PMS). However, the rate constant of the phenol degradation decreased slightly to 0.15 min^{-1} at the molar ratio of 1:32 (phenol/PMS). This phenomenon may be explained by following equations. The Eqs. (1)–(3) (Duan et al., 2016; Khan et al., 2017; Wang et al., 2017) reveal the excess PMS may react with sulfate radicals and hydroxyl radicals to decrease the oxidative ability of the UV/PMS/CNT-TiO_2 system. Furthermore, the SO_5•$^-$ with lower oxidative potential (E_0 = 1.1 V) which is activated by HSO_5^- and SO_5^{2-} will be quenched by SO_4•$^-$ (E_0 > 3.0 V) in the reaction process. Thus, the molar ratio of 1:16 (phenol/PMS) was used in the following experiments. The corresponding actual usage of PMS was 0.087 mmol/L.

$$HSO_5^- + SO_4\cdot^- \rightarrow SO_4^{2-} + SO_5\bullet^- + H^+$$

$$k < 1 \times 10^5\ M^{-1}\cdot s^{-1} \quad (1)$$

$$HSO_5^- + \bullet OH \rightarrow SO_5\bullet^- + H_2O$$

$$k = 1.7 \times 10^7\ M^{-1}\cdot s^{-1} \quad (2)$$

$$SO_5^{2-} + \bullet OH \rightarrow SO_5\bullet^- + OH^-$$

$$k = 2.1 \times 10^9\ M^{-1}\cdot s^{-1} \quad (3)$$

3.4 Reactive species in UV/PMS/CNT-TiO_2 system

It was reported that the reaction rates of SO_4•$^-$ and •OH with methanol (MeOH) are 3.2 × 10^6 $M^{-1}\cdot s^{-1}$ and 9.7 × 10^8 $M^{-1}\cdot s^{-1}$, respectively (Duan et al., 2016). The reaction rate of *tert*-butyl alcohol (TBA) with hydroxyl radical (3.8–7.6 × 10^8 $M^{-1}\cdot s^{-1}$) was over 1000 times faster than that of TBA with sulfate radical (4.0–9.1 × 10^5 $M^{-1}\cdot s^{-1}$) (Anipsitakis and Dionysiou, 2004). The MeOH and TBA were selected to differentiate the sulfate radicals from hydroxyl radicals in quenching experiments. As shown in Fig. 9, the removal of phenol decreased from 100% to 67% at the molar ratio of 500:1 (TBA/PMS). These results suggested the presence of hydroxyl radical which could be generated from the photocatalysis and PMS activation via UV energy, according to Eqs. (4) and (5) (Wang et al., 2017). When the MeOH (the molar ratio of MeOH/PMS = 500:1) was added into the UV/PMS/CNT-TiO_2 system, the removal of phenol decreased from 100% to 57%, indicating the production of sulfate radical in this reaction

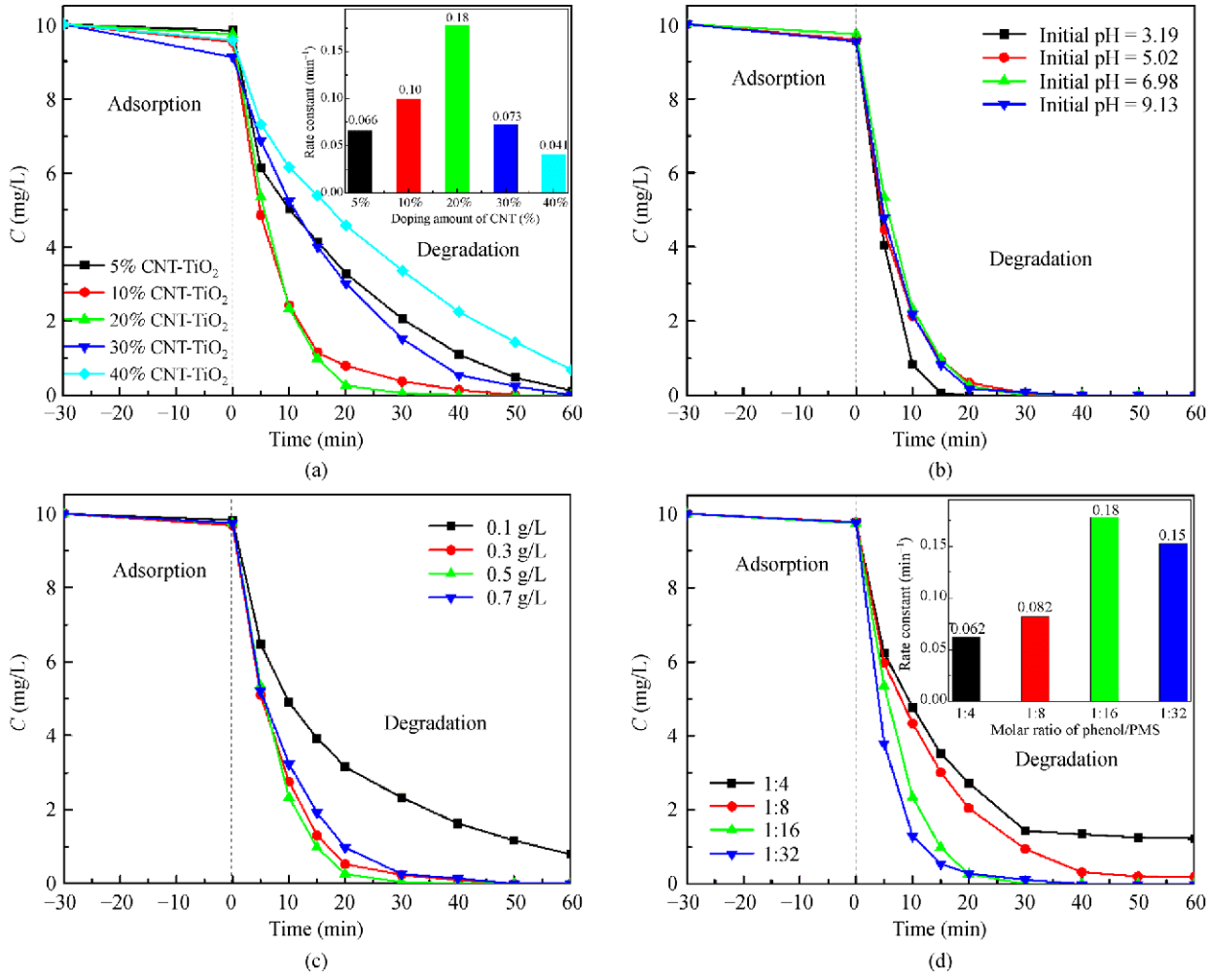

Fig. 8 The effect of different doping amounts of CNT in composite (a), initial pH (b), composite dosage (c) and the molar ratio of phenol/PMS (d) in UV/PMS/composite system ([phenol] = 10 mg/L, the doping amount of CNT = 5%–20%, [catalyst] = 0.1–0.7 g/L, the molar ratio of phenol/PMS = 1:4–1:32, initial pH = 3.19–9.13, t = 30°C).

(Eqs. (5), (6) and (7)). According to previous researches (Zhou et al., 2015, 2017), $^1O_2$ probably existed in the reaction system. Therefore, the L-histidine was selected as the scavenger for the quenching of $^1O_2$ (Lee et al., 2016; Lu et al., 2018). Both L-histidine (0.1 mmol/L) and MeOH (MeOH/phenol = 500) are added into UV/PMS/CNT-TiO_2 system to quench the $^1O_2$, •OH and SO_4•$^-$. The corresponding removal of phenol decreased from 100% to 5% in 30 min. It seems consistent with the previous studies (Zhang et al., 2009; Yun et al., 2018). The generation of $^1O_2$ may be responsible for the nonradical reaction pathway in the activation of PMS or the photocatalysis process in the UV/PMS/CNT-TiO_2 system. The above results indicated that $^1O_2$ and •OH, as the major oxidants, were responsible for the phenol degradation. Meanwhile, the SO_4•$^-$ was also involved in the reaction to remove organic pollutants.

$$h^+(TiO_2) + H_2O \rightarrow \bullet OH + H^+ \quad (4)$$

$$HSO_5^-/SO_5^{2-} + h\nu \rightarrow SO_4\bullet^- + \bullet OH \quad (5)$$

$$HSO_5^- + e^- \rightarrow SO_4\bullet^- + OH^- \quad (6)$$

$$HSO_5^- + e^- \rightarrow \bullet OH + SO_4^{2-} \quad (7)$$

The EPR technique was used to confirm the active radicals generated in the UV/PMS/CNT-TiO_2 system. The DMPO (Zhang et al., 2017) and TMP are generally considered as good probes for •OH/SO_4•$^-$ and $^1O_2$. Hence, as shown in Fig. 10, the EPR signals of DMPO-•OH (a_N = a_H = 14.9 G) and DMPO-SO_4•$^-$ (a_N = 13.8 G, a_H = 10.1 G, a_H = 1.42 G, a_H = 0.83 G) (Gao et al., 2018) were detected in the UV/PMS/CNT-TiO_2 system, suggesting the genera-

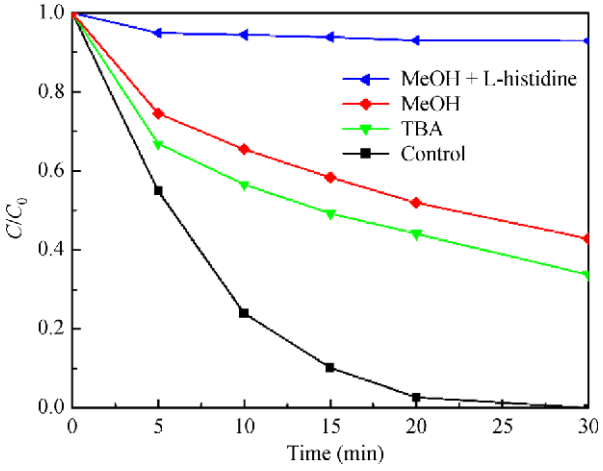

Fig. 9 Phenol degradation by the UV/PMS/20%CNT-TiO_2 system in the presence of TBA, MeOH and L-histidine. ([phenol] = 10 mg/L, [catalyst] = 0.5 g/L, the molar ratio of phenol/PMS = 1:16, the molar ratio of MeOH/PMS = TBA/PMS = 500, [L-histidine] = 0.1 mmol/L, initial pH = 6.98, t = 30°C).

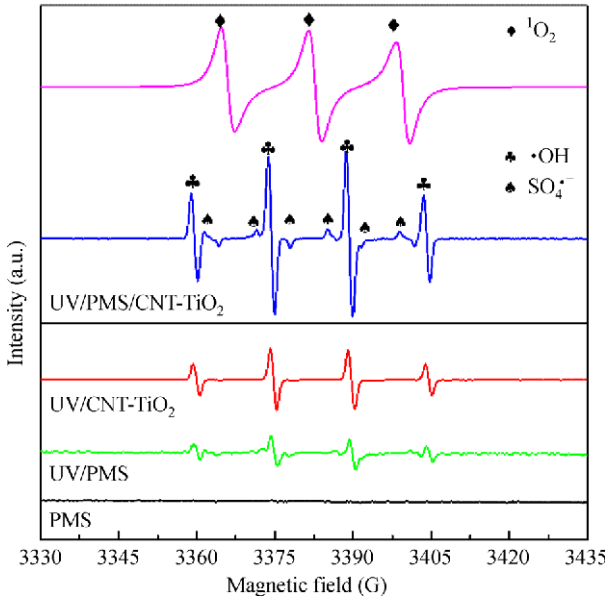

Fig. 10 The EPR spectra for $SO_4^{\bullet-}$, •OH and $^1O_2$ in the various systems. ([catalyst] = 0.5 g/L, the molar ratio of phenol/PMS = 1:16, [DMPO] = 50 mmol/L, [TMP] = 50 mmol/L, t = 25°C).

tion of •OH and $SO_4^{\bullet-}$. In the presence of TMP, the typical three-line EPR spectrum with equal intensities adducts appeared, indicating the existence of $^1O_2$ in the system.

3.5 Mechanism of PMS activation on UV assisted CNT-TiO_2 system

The PL was used to study the separation efficiency of photoinduced electrons and holes of the composite catalyst. The lower intensity of fluorescence peak means better separation of photoinduced electron-hole pairs. As shown in Fig. 11, the fluorescence absorption intensity of TiO_2 catalyst alone was much stronger than that of 20% CNT-TiO_2 composite catalyst (no peaks for CNT), whose fluorescence spectrum absorption peak centered at around 450 nm with excitation wavelength of 320 nm. As expected, the PL intensity of 20%CNT-TiO_2 samples showed a significant decrease compared with TiO_2 alone. The results demonstrated that the 20%CNT-TiO_2 enhanced the separation of photoinduced electron-hole pairs due to the good electron transfer ability of composite, which was beneficial to the activation of PMS (Fujihara et al., 2000; Yao et al., 2008).

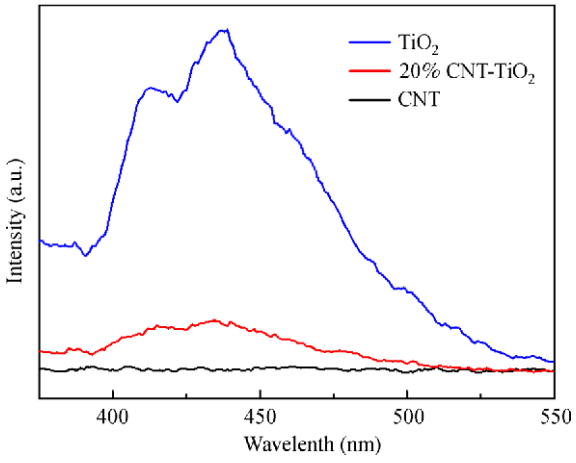

Fig. 11 The PL spectra of TiO_2, CNT and 20%CNT-TiO_2 composite.

Furthermore, in order to investigate the electron transfer capability of 20%CNT-TiO_2/PMS under the UV-light assistance, the EIS of 20%CNT-TiO_2 was performed. The diameter of semicircle can reflect the resistance (R_{CT}) of charge transfer. As a general rule, the bigger arc diameter means a higher charge transfer. As shown in Fig. 12, the order of the R_{CT} of three systems was UV/PMS/20%CNT-TiO_2 < PMS/20%CNT-TiO_2 < UV/20% CNT-TiO_2. The presence of PMS in the UV/20%CNT-TiO_2 could greatly promote the photoinduced electron-hole pairs separation and enhance the charge transfer. Moreover, the R_{CT} in the UV/PMS/20%CNT-TiO_2 system was lower than that in the PMS/20%CNT-TiO_2 system, which suggested the significant role of UV-light assistance in the UV/PMS/20% CNT-TiO_2 system. The photoinduced electrons were supplied to PMS to produce sulfate radicals via nonradical pathway (Lee et al., 2015; Lim et al., 2018). Therefore, the better electron transfer performance facilitated greatly the activation of PMS to improve the catalytic degradation ability in the UV/PMS/20%CNT-TiO_2 system (He and Mansfeld, 2009; Wang et al., 2017).

Based on the above results, a hypothesis of three reaction pathways in the UV/PMS/20%CNT-TiO_2 system

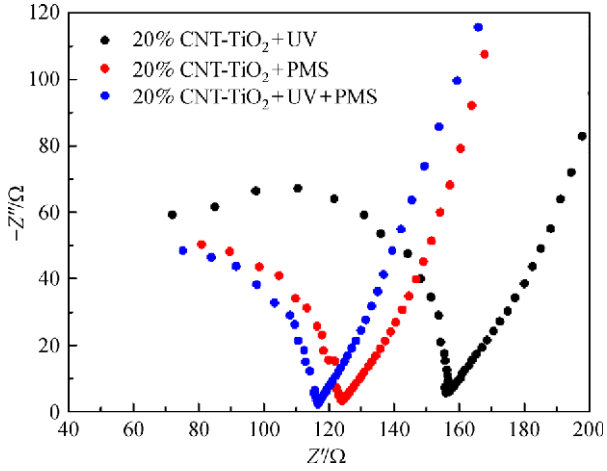

Fig. 12 Electrochemical impedance spectroscopy Nynquist plots of 20%CNT-TiO_2 /UV, 20%CNT-TiO_2/PMS and UV/PMS/20%CNT-TiO_2 reaction system. (Scan rate: 5 mV/s, frequency range 0.1–1.0 × 10^6 Hz, [Na_2SO_4] = 0.01 mol/L, [PMS] = 0.087 mmol/L).

was proposed as shown in Fig. 13. First, the PMS was activated by UV light directly to generate •OH and SO_4•$^-$ owing to the breaking of O – O bond by light-energy radiation. Secondly, the TiO_2 was excited by UV-light to produce photoinduced electron-hole pairs, which subsequently reacted with H_2O/O_2 to generate •OH or $^1O_2$. Thirdly, the photoinduced electrons led to the effective activation of PMS, which could transfer from TiO_2 via CNT to transform PMS into various radicals including SO_4•$^-$, •OH and $^1O_2$. The catalytic performance of the UV/PMS/20%CNT-TiO_2 system could be enhanced significantly owing to these radicals.

4 Conclusions

This study demonstrated that the 20%CNT-TiO_2 composite catalyst can efficiently activate PMS to generate SO_4•$^-$, •OH and $^1O_2$ with the assistance of UV-light. The UV/PMS/20%CNT-TiO_2 system exhibited an outstanding performance for the degradation of phenol due to a remarkable synergy effect. Furthermore, the high efficiency of electron transfer between the CNT-TiO_2 composite and PMS was crucial for the PMS activation. Almost 100% phenol could be removed within 20 min. The kinetic rate constant of phenol degradation in the

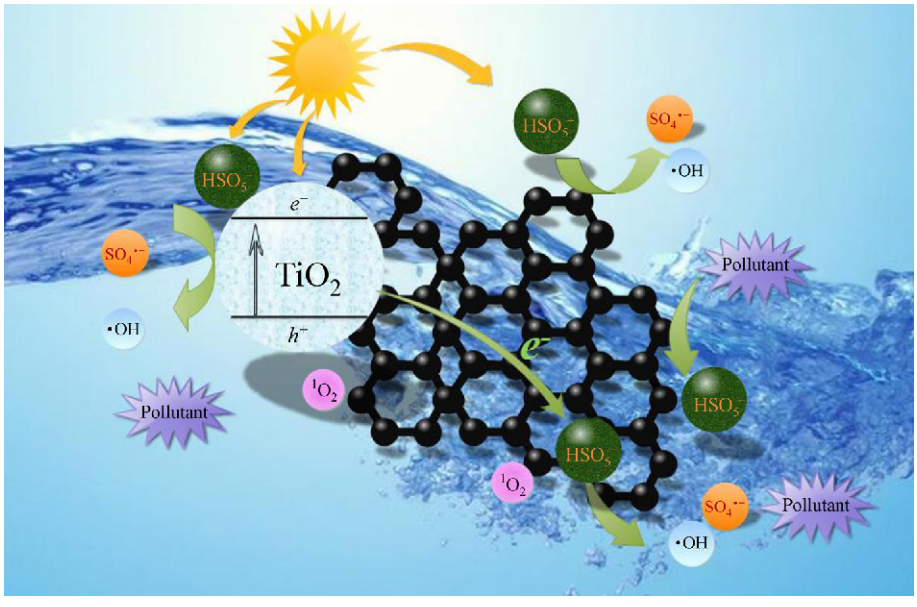

Fig. 13 A hypothetical reaction mechanism diagram of the UV/PMS/20%CNT-TiO_2 system.

UV/PMS/20%CNT-TiO_2 system was 0.18 min^{-1}, which was about 23.7 times that in the PMS/Co_3O_4 system. This work provided another perspective for the future technical complementarity to achieve the efficient PMS activation for organic pollutant degradation.

Acknowledgements This work was supported by National Natural Science Foundation of China (Grant No. 21590813), Department of Science and Technology of Dalian (No. 2018J11CY012), the Program of Introducing Talents of Discipline to Universities (No. B13012), and program for Changjiang Scholars and Innovative Research Team in University (No. IRT_13R05).

References

Anipsitakis G P, Dionysiou D D (2003). Degradation of organic contaminants in water with sulfate radicals generated by the conjunction of peroxymonosulfate with cobalt. Environmental Science & Technology, 37(20): 4790–4797

Anipsitakis G P, Dionysiou D D (2004). Radical generation by the interaction of transition metals with common oxidants. Environmental Science & Technology, 38(13): 3705–3712

Cao F, Guo Y, Zheng S F, Wu X, Jiang L, Bi R, Wan L, Maier J (2010). Symbiotic coaxial nanocables: Facile synthesis and an efficient and elegant morphological solution to the lithium storage problem. Chemistry of Materials, 22(5): 1908–1914

Chen Q, Ji F, Guo Q, Fan J, Xu X (2014). Combination of heterogeneous Fenton-like reaction and photocatalysis using Co-TiO_2 nanocatalyst for activation of $KHSO_5$ with visible light irradiation at ambient conditions. Journal of Environmental Sciences- China, 26(12): 2440–2450

Dikdim J M D, Gong Y, Noumi G B, Sieliechi J M, Zhao X, Ma N, Yang M, Tchatchueng J B (2019). Peroxymonosulfate improved photocatalytic degradation of atrazine by activated carbon/graphitic carbon nitride composite under visible light irradiation. Chemosphere, 217: 833–842

Duan X, Ao Z, Zhou L, Sun H, Wang G, Wang S (2016). Occurrence of radical and nonradical pathways from carbocatalysts for aqueous and nonaqueous catalytic oxidation. Applied Catalysis B: Environmental, 188: 98–105

Duan X, Sun H, Kang J, Wang Y, Indrawirawan S, Wang S (2015a). Insights into heterogeneous catalysis of persulfate activation on dimensional-structured nanocarbons. ACS Catalysis, 5(8): 4629–4636

Duan X, Sun H, Wang Y, Kang J, Wang S (2015b). N-doping-induced nonradical reaction on single-walled carbon nanotubes for catalytic phenol oxidation. ACS Catalysis, 5(2): 553–559

Fujihara K, Izumi S, Ohno T, Matsumura M (2000). Time-resolved photoluminescence of particulate TiO_2 photocatalysts suspended in aqueous solutions. Journal of Photochemistry and Photobiology A Chemistry, 132(1–2): 99–104

Gao Y, Zhu Y, Lyu L, Zeng Q, Xing X, Hu C (2018). Electronic structure modulation of graphitic carbon nitride by oxygen doping for enhanced catalytic degradation of organic pollutants through peroxymonosulfate activation. Environmental Science & Technology, 52(24): 14371–14380

Ghanbari F, Moradi M (2017). Application of peroxymonosulfate and its activation methods for degradation of environmental organic pollutants. Chemical Engineering Journal, 310: 41–62

Golshan M, Kakavandi B, Ahmadi M, Azizi M (2018). Photocatalytic activation of peroxymonosulfate by TiO_2 anchored on cupper ferrite (TiO_2@$CuFe_2O_4$) into 2,4-D degradation: Process feasibility, mechanism and pathway. Journal of Hazardous Materials, 359: 325–337

Guo X, Zhu Y, Han W, Fan X, Li Y, Zhang F, Zhang G, Peng W, Wang S (2019). Nitrogen-doped graphene quantum dots decorated graphite foam as ultra-high active free-standing electrode for electrochemical hydrogen evolution and phenol degradation. Chemical Engineering Science, 194(SI): 54–57

Guo Y, Zeng Z, Li Y, Huang Z, Cui Y (2018). In-situ sulfur-doped carbon as a metal-free catalyst for persulfate activated oxidation of aqueous organics. Catalysis Today, 307: 12–19

He Z, Mansfeld F (2009). Exploring the use of electrochemical impedance spectroscopy (EIS) in microbial fuel cell studies. Energy & Environmental Science, 2(2): 215–219

Hu L, Yang X, Dang S (2011). An easily recyclable Co/SBA-15 catalyst: Heterogeneous activation of peroxymonosulfate for the degradation of phenol in water. Applied Catalysis B: Environmental, 102(1–2): 19–26

Khan A, Liao Z, Liu Y, Jawad A, Ifthikar J, Chen Z (2017). Synergistic degradation of phenols using peroxymonosulfate activated by CuO-Co_3O_4@MnO_2 nanocatalyst. Journal of Hazardous Materials, 329: 262–271

Lee H, Kim H I, Weon S, Choi W, Hwang Y S, Seo J, Lee C, Kim J H (2016). Activation of persulfates by graphitized nanodiamonds for removal of organic compounds. Environmental Science & Technology, 50(18): 10134–10142

Lee H, Lee H J, Jeong J, Lee J, Park N B, Lee C (2015). Activation of persulfates by carbon nanotubes: Oxidation of organic compounds by nonradical mechanism. Chemical Engineering Journal, 266: 28–33

Lei Y, Chen C S, Tu Y J, Huang Y H, Zhang H (2015). Heterogeneous degradation of organic pollutants by persulfate activated by CuO-Fe_3O_4: Mechanism, stability, and effects of pH and bicarbonate Ions. Environmental Science & Technology, 49(11): 6838–6845

Liang H, Sun H, Patel A, Shukla P, Zhu Z, Wang S (2012). Excellent performance of mesoporous Co_3O_4/MnO_2 nanoparticles in heterogeneous activation of peroxymonosulfate for phenol degradation in aqueous solutions. Applied Catalysis B: Environmental, 127: 330–335

Lim J, Kwak D Y, Sieland F, Kim C, Bahnemann D W, Choi W (2018). Visible light-induced catalytic activation of peroxymonosulfate using heterogeneous surface complexes of amino acids on TiO_2. Applied Catalysis B: Environmental, 225: 406–414

Lu S, Wang G, Chen S, Yu H, Ye F, Quan X (2018). Heterogeneous activation of peroxymonosulfate by $LaCo_{1-x}Cu_xO_3$ perovskites for degradation of organic pollutants. Journal of Hazardous Materials, 353: 401–409

Matafonova G, Batoev V (2018). Recent advances in application of UV light-emitting diodes for degrading organic pollutants in water through advanced oxidation processes: A review. Water Research, 132: 177–189

Ren Y, Lin L, Ma J, Yang J, Feng J, Fan Z (2015). Sulfate radicals induced from peroxymonosulfate by magnetic ferrospinel MFe_2O_4(M = Co, Cu, Mn, and Zn) as heterogeneous catalysts in the water. Applied Catalysis B: Environmental, 165: 572–578

Shukla P, Fatimah I, Wang S, Ang H M, Tadé M O (2010). Photocatalytic generation of sulphate and hydroxyl radicals using zinc oxide under low-power UV to oxidise phenolic contaminants in wastewater. Catalysis Today, 157(1–4): 410–414

Taha S M, Amer M E, Elmarsafy A M, Elkady M Y, Chovelon J M (2016). Degradation of boscalid by nitrogen-doped/undoped TiO_2 and persulfate ions using different activation conditions and the identification of its main degradation products using LC/MS/MS. Chemical Engineering Journal, 288: 845–857

Verma S, Nakamura S, Sillanpää M (2016). Application of UV-C LED activated PMS for the degradation of anatoxin-a. Chemical Engineering Journal, 284: 122–129

Wang G, Chen S, Quan X, Yu H, Zhang Y (2017). Enhanced activation of peroxymonosulfate by nitrogen doped porous carbon for effective removal of organic pollutants. Carbon, 115: 730–739

Wang G, Nie X, Ji X, Quan X, Chen S, Wang H, Yu H, Guo X (2019). Enhanced heterogeneous activation of peroxymonosulfate by Co and N codoped porous carbon for degradation of organic pollutants: the synergism between Co and N. Environmental Science. Nano, 6(2): 399–410

Wang H, Liu S, Wang H, Jiang W (2010). Solar photocatalytic decomposition of two azo dyes on multi walled carbon nanotubes (MWCNTs)/TiO_2 composites. Frontiers of Environmental Science & Engineering in China, 4(3): 311–320

Wang J, Wang S (2018). Activation of persulfate (PS) and peroxymonosulfate (PMS) and application for the degradation of emerging contaminants. Chemical Engineering Journal, 334: 1502–1517

Yang M Q, Zhang N, Xu Y J (2013). Synthesis of fullerene-, carbon nanotube-, and graphene-TiO_2 nanocomposite photocatalysts for selective oxidation: A comparative study. ACS Applied Materials & Interfaces, 5(3): 1156–1164

Yang Q, Choi H, Chen Y, Dionysiou D D (2008). Heterogeneous activation of peroxymonosulfate by supported cobalt catalysts for the degradation of 2,4-dichlorophenol in water: The effect of support, cobalt precursor, and UV radiation. Applied Catalysis B: Environmental, 77(3–4): 300–307

Yao Y, Li G, Ciston S, Lueptow R M, Gray K A (2008). Photoreactive TiO_2/carbon nanotube composites: Synthesis and reactivity. Environmental Science & Technology, 42(13): 4952–4957

Yu H, Quan X, Chen S, Zhao H (2007). TiO_2-multiwalled carbon nanotube heterojunction arrays and their charge separation capability. Journal of Physical Chemistry, 111(35): 12987–12991

Yun E T, Lee J H, Kim J, Park H D, Lee J (2018). Identifying the nonradical mechanism in the peroxymonosulfate activation process: Singlet oxygenation versus mediated electron transfer. Environmental Science & Technology, 52(12): 7032–7042

Zhang A, He Y, Chen Y, Feng J, Huang N, Lian F (2018). Degradation of organic pollutants by Co_3O_4-mediated peroxymonosulfate oxidation: Roles of high-energy exposed TiO_2 support. Chemical Engineering Journal, 334: 1430–1439

Zhang D, Qiu R, Song L, Eric B, Mo Y, Huang X (2009). Role of oxygen active species in the photocatalytic degradation of phenol using polymer sensitized TiO_2 under visible light irradiation. Journal of Hazardous Materials, 163(2–3): 843–847

Zhang X, Feng M, Wang L, Qu R, Wang Z (2017). Catalytic degradation of 2-phenylbenzimidazole-5-sulfonic acid by peroxymonosulfate activated with nitrogen and sulfur co-doped CNTs-COOH loaded $CuFe_2O_4$. Chemical Engineering Journal, 307: 95–104

Zhang Y, Tang Z R, Fu X, Xu Y J (2010). TiO_2-graphene nanocomposites for gas-phase photocatalytic degradation of volatile aromatic pollutant: Is TiO_2-graphene truly different from other TiO_2-carbon composite materials? ACS Nano, 4(12): 7303–7314

Zhang Y, Tang Z R, Fu X, Xu Y J (2011). Engineering the unique 2D mat of graphene to achieve graphene-TiO_2 nanocomposite for photocatalytic selective transformation: what advantage does graphene have over its forebear carbon nanotube? ACS Nano, 5(9): 7426–7435

Zhao Q, Mao Q, Zhou Y, Wei J, Liu X, Yang J, Luo L, Zhang J, Chen H, Chen H, Tang L (2017). Metal-free carbon materials-catalyzed sulfate radical-based advanced oxidation processes: A review on heterogeneous catalysts and applications. Chemosphere, 189: 224–238

Zhou Y, Jiang J, Gao Y, Ma J, Pang S Y, Li J, Lu X T, Yuan L P (2015). Activation of peroxymonosulfate by benzoquinone: A novel nonradical oxidation process. Environmental Science & Technology, 49(21): 12941–12950

Zhou Y, Jiang J, Gao Y, Pang S Y, Yang Y, Ma J, Gu J, Li J, Wang Z, Wang L H, Yuan L P, Yang Y (2017). Activation of peroxymonosulfate by phenols: Important role of quinone intermediates and involvement of singlet oxygen. Water Research, 125: 209–218